Journal of Power Sources 189 (2009) 1204–1211

Contents lists available at ScienceDirect

Journal of Power Sources

journal homepage: www.elsevier.com/locate/jpowsour

Electrochemical behavior and application of lead–lanthanum alloys for positive grids of lead-acid batteries☆

Aiju Li[a], Yiman Cheni[a], Hongyu Chen[a,*], Dong Shu[a], Weishan Li[a], Hui Wang[b], Chuanlong Dou[b], Wei Zhang[b], Shun Chen[b]

[a] School of Chemistry and Environment, South China Normal University, Key Lab of Electrochemical Technology on Energy Storage and Power Generation in Guangdong Universities, Guangzhou, Guangdong 510006, China
[b] Zhuzhou Smelter Group Co., Ltd., Zhuzhou, Hunan 412004, China

ARTICLE INFO

Article history:
Received 27 May 2008
Received in revised form
22 November 2008
Accepted 22 December 2008
Available online 30 December 2008

Keywords:
Lead-acid battery
Grid
Lead–lanthanum alloy
Electrochemical behavior

ABSTRACT

The effects of different lanthanum content (0, 0.00600, 0.0112, 0.0195 and 0.0540 wt.%) on the electrochemical behavior of lead–lanthanum alloy in sulfuric acid solutions were investigated by linear potential sweep (LSV), cyclic voltammetry (CV), and electrochemical impedance spectroscopy (EIS). The morphology of the corrosion layer and corrosion section of Pb and Pb–La alloys were analyzed by scanning electron microscope (SEM) after corrosion testing. It was found that the addition of La inhibits the oxygen evolution reaction on the surface of Pb alloy electrodes, and La amounts of 0.00600 and 0.0540 wt.% in Pb–La alloy electrodes can lead to a more effective inhibition. The results of the LSV, CV and EIS experiments show that the addition of La can inhibit the growth of the anodic Pb(II) oxides and PbO_2 film. The resistance of the anodic film on the Pb–La electrodes is much lower than that on the Pb electrode. SEM for the corrosion layer indicates that the corrosion product on pure Pb and Pb–0.0195% La alloy is uniform and compact. The corrosion products on the alloys with La contents of 0.00600, 0.0112 and 0.0540 are loose and porous that the active materials can easily sit in the apertures to contact the grid surface intimately with the effective. The results demonstrate that Pb–La alloys show the potential for application as the positive grid material in maintenance-free lead-acid batteries.

1. Introduction

Up to now, lead-acid batteries are still widely used due to their high performance/price ratio, safety and reliability [1–3]. Two main types of positive grid, the low-antimony grid and the lead–calcium grid are widely used in lead-acid batteries [4–7]. However, the lower over-potential of hydrogen evolution on the antimony surface leads to high gas evolution and self-discharge during the charge/discharge process, so that regular maintenance of the battery is required [8–10]. The lead–calcium grid has good maintenance-free performance but has a short deep-discharge cycle life. In the deep-discharge process, a Pb(II) ($PbO + PbO{\cdot}PbSO_4$) film with high resistivity grows more easily on the positive grid alloys, seriously shortening the cycle life [11].

Many researchers aim to discover a suitable additive to generate alloys which eliminate the detrimental influences of Pb–Sb and Pb–Ca alloys (such as Sr, Cd and Ag), [12–14]. They all have improved some properties of the alloys. However, cadmium can pollute the environment heavily and be harmful to the health of the workers; Ag is too expensive compared to the above-mentioned elements. Rare earth elements are often used in the metallurgy industry to improve the fine crystal grain structure of alloys in order to enhance the corrosion and abrasion resistance of alloys. Recently, it has been reported that the performance of lead alloys can be improved by adding some rare earth elements such as Sm, Ce, Pr, Gd, La and Y [15–20]. These results indicated that rare earth elements are beneficial to the grid properties of lead-acid batteries.

In this paper, a novel Pb–La alloy, and the effects of varying the weight percentage of La were investigated as a positive grid for valve-regulated lead-acid batteries. The characteristics of Pb–La alloys and the optimum La content were also investigated.

2. Experimental

Pb–La binary alloys (La content of 00, 0.00600, 0.0112, 0.0195 and 0.0540 wt.%) were processed by melting the mixtures of pure lead (99.994%) and pure lanthanum (99.95%) in an electrical furnace under an argon gas atmosphere at 800 °C for 15 min, cooling down to room temperature, and served as working electrodes, in the form of rods with a geometric area of 0.3 cm^2. The contents of the La were obtained by the ICP iCAP6500 of the thermo-electron corporation.

☆ This paper was presented at 12th Asian Battery Conference (12ABC).

* Corresponding author. Tel.: +86 20 39310183; fax: +86 20 39310183.
E-mail address: battery@scnu.edu.cn (H. Chen).

0378-7753/$ – see front matter © 2009 Elsevier B.V. All rights reserved.
doi:10.1016/j.jpowsour.2008.12.093

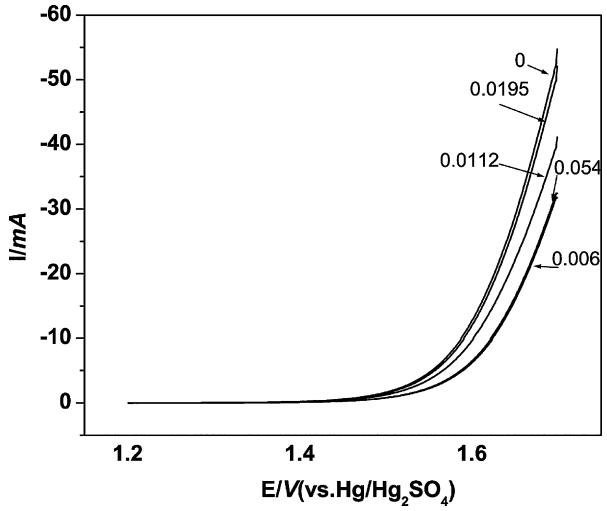

Fig. 1. Oxygen evolution on Pb alloy electrodes with different amounts of La in 1.28 g cm^{-3} H_2SO_4 (scan rate = 1 mV s^{-1}).

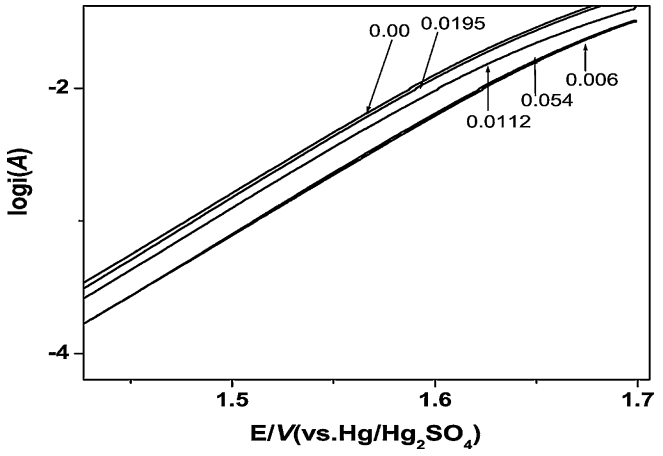

Fig. 2. Tafel plots of oxygen evolution on Pb alloy electrodes with different amounts of La.

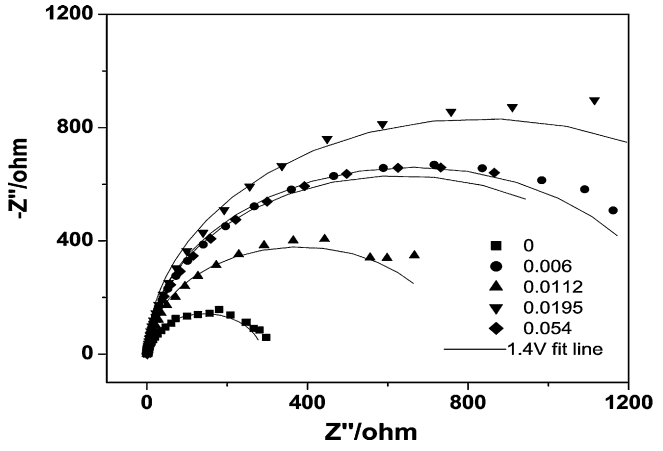

Fig. 3. Electrochemical impedance spectra of the oxygen evolution reaction on Pb alloy electrodes with different amounts of La in 1.28 g cm^{-3} H_2SO_4 solution at 1.4 V.

Electrochemical tests were performed in a three-electrode configuration using an Autolab PGSTAT-30 potentionstat/galvanostat (ECO Echemie B.V., Holland). The counter and reference electrodes were a platinum plate (0.3 cm^2) and Hg/Hg_2SO_4 electrode (1.28 g cm^{-3} H_2SO_4 solution, E = +0.658 vs. SHE), respectively. All potentials are reported with respect to this reference electrode. The electrolyte was 1.28 g cm^{-3} sulfuric acid solution, which was prepared from analytical grade reagent and maintained at 25 °C.

Prior to each experiment, all working electrodes were mechanically polished successively with fine 2000-grade SiC emery paper. The polished lead electrode was reduced at −1.2 V to eliminate oxides on the electrode surface.

Corrosion tests were conducted in assembled cells using Pb–La with different amounts of La as the positive electrode and Pb as the negative electrode. Test cells were charged for 1 h and then discharged to open potential repeatedly. This experiment lasted for 50 days. Each corroded electrode was then observed by scanning electron microscopy (SEM), after washing and drying.

3. Results and discussion

3.1. Oxygen evolution

In order to understand the anodic behavior of oxygen evolution on the alloys, the anodic polarization curves were recorded by sweeping the potential negatively after keeping the potential at 1.7 V for 1 h in 1.28 g cm^{-3} sulfuric acid solution to form a layer of lead oxide. The results are shown in Fig. 1. The corresponding Tafel plots are presented in Fig. 2, and the kinetic parameters of the oxygen evolution reaction are listed in Table 1. It can be seen that the a value of Pb–0.0195 wt.% La binary alloy is almost the same as that of pure lead alloy. This suggests that this particular content of La (0.0195 wt.%) has little influence on the oxygen evolution reaction. However, when the La content is greater than this amount, the a value is higher than that of pure lead. This indicates that the La in the alloys inhibits the oxygen evolution reaction; however, it is not linear with the amount of La added. The Pb–La alloys with 0.00600 and 0.0540 wt.% La content show slower oxygen evolution rates.

Table 1
Kinetic parameters of the oxygen evolution reaction on Pb alloy electrodes with different amounts of La obtained by LSV method.

	La (wt.%)				
	0.00	0.006	0.0112	0.0195	0.054
a	1.8147	1.8306	1.8244	1.8137	1.8341
b	0.1115	0.1047	0.1099	0.1094	0.1065

Fig. 3 shows the electrochemical impedance spectra of Pb–La alloys obtained at 1.4 V. The electrode was pretreated, using the same method as that in Fig. 1. The AC amplitude was 5 mV and the frequency was in the range of 10×10^5–10 Hz. The charge transfer resistance and the double layer capacitance were obtained by assuming the equivalent circuit of Fig. 4 and are listed in Table 2. R_s is the electrolyte resistance, R_{ct} is the electrochemical reaction resistance, and C is the capacity of the electric double-layer. The plots for the five electrodes are similar and exhibit a semicircular part at high frequency that indicates control by electron transfer. The semicircular radius of the plots for each of the Pb–0.00600% La, Pb–0.0112% La, Pb–0.0195% La and Pb–0.0540% La electrodes is

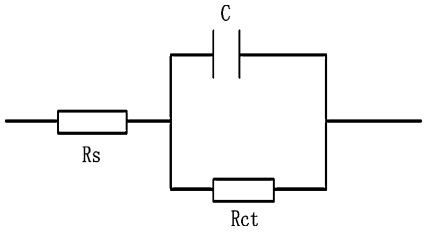

Fig. 4. The equivalent circuit of Fig. 3.

Table 2
Change transfer resistance R_{ct} and double layer capacitance for the oxygen evolution reaction on the Pb–La alloys at 1.4 V.

	La (wt.%)				
	0.00	0.006	0.0112	0.0195	0.054
R_{ct} (Ω cm^2)	285	1320	757	1640	1260
Capacitance (mF)	10.21	4.32	7.92	6.00	7.34

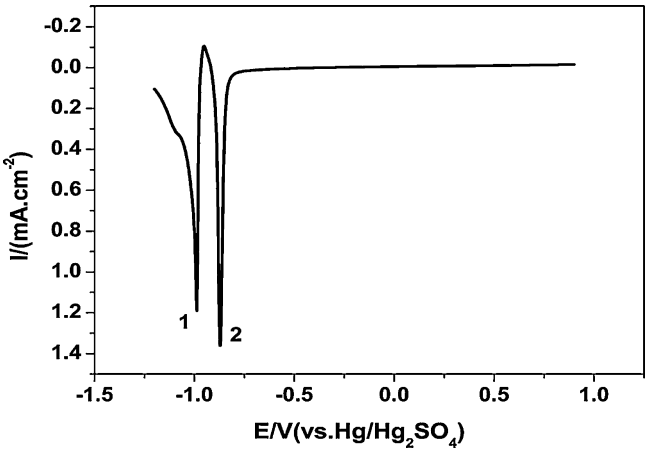

Fig. 5. Voltammograms of anodic films formed on Pb alloy electrode at 0.9 V for 1 h in 1.28 g cm^{-3} H_2SO_4 (scan rate = 1 mV s^{-1}).

much larger than that of the Pb electrode. The R_{ct} of Pb–La electrode is much larger than that of the pure Pb electrodes. It can be seen that the impedance behavior is significantly influenced by the addition of La. This suggests that the oxygen evolution reaction is inhibited on the surface of Pb–La alloys due to the addition of La.

3.2. Linear sweep voltammetry

The electrodes were kept at 0.9 and 1.3 V for 1 h and then swept negatively to −1.2 V at a rate of 1 mV s^{-1} in 1.28 g cm^{-3} H_2SO_4 solution. The value of 0.9 V is close to the potential that the positive grids experience from the deep-discharge, and 1.3 V is close to the potential of the float-charge.

Figs. 5 and 6 show the typical voltammograms of anodic films on Pb alloy electrode. The voltammograms of other electrodes have similar shapes to Figs. 5 and 6. As can be seen in Fig. 6, peak 1 corresponds to the reduction of $PbSO_4$ to Pb, peak 2 to the reduction of Pb(II) oxides to Pb, and peak 3 to the reduction of PbO_2 to $PbSO_4$. Figs. 7–9 show the reduction current of peaks 2 (Pb(II)/Pb) and 3 (PbO_2/$PbSO_4$), for Pb and Pb–La electrodes. It can be seen from Figs. 7–9 that the peak 2 current for Pb–La electrodes is lower than that for Pb electrodes. A possible explanation is that lower amounts of anodic Pb(II) oxide and PbO_2 films are formed on the Pb–La electrodes, and the shape of Fig. 8 (for peak 3) is similar to Figs. 7 and 9. They all show an anomalous "h" shape. This suggests that adding La can inhibit the growth of both the anodic Pb(II) oxides film and

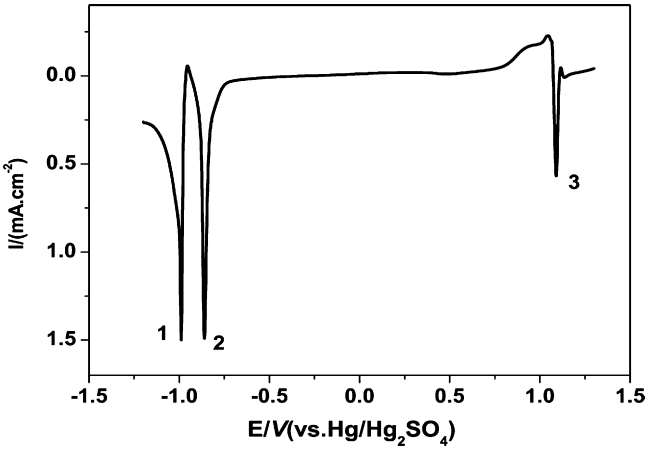

Fig. 6. Voltammograms of anodic films formed on Pb alloy electrode at 1.3 V for 1 h in 1.28 g cm^{-3} H_2SO_4 (scan rate = 1 mV s^{-1}).

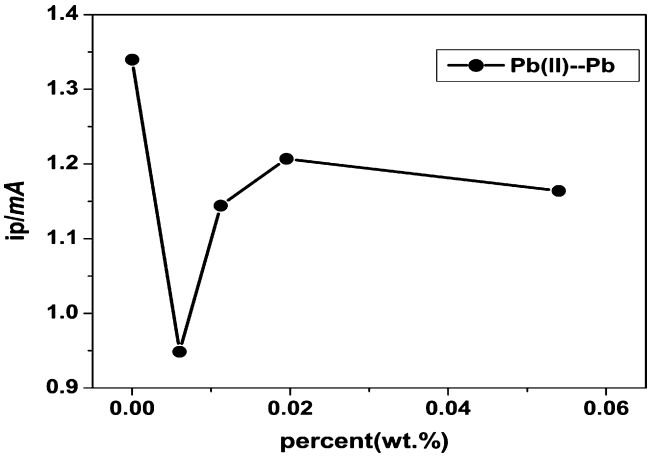

Fig. 7. Relationship between peak current and La weight percent (Fig. 5 peak 2).

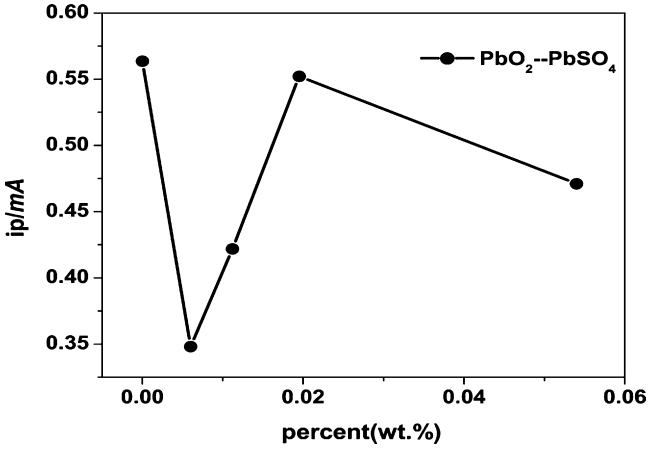

Fig. 8. Relationship between peak current and La weight percent (Fig. 6 peak 3).

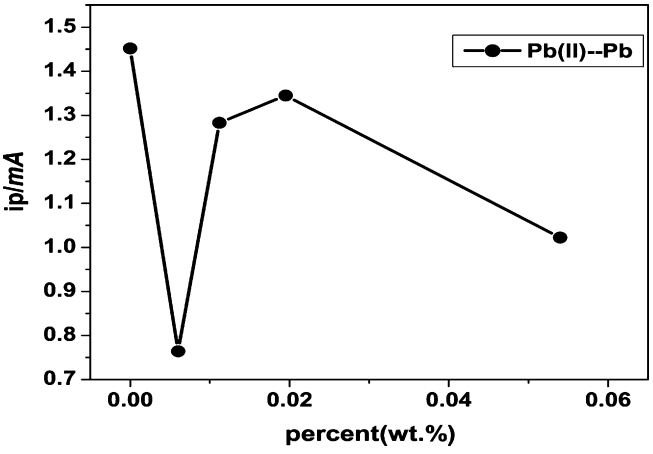

Fig. 9. Relationship between peak current and La weight percent (Fig. 6 peak 2).

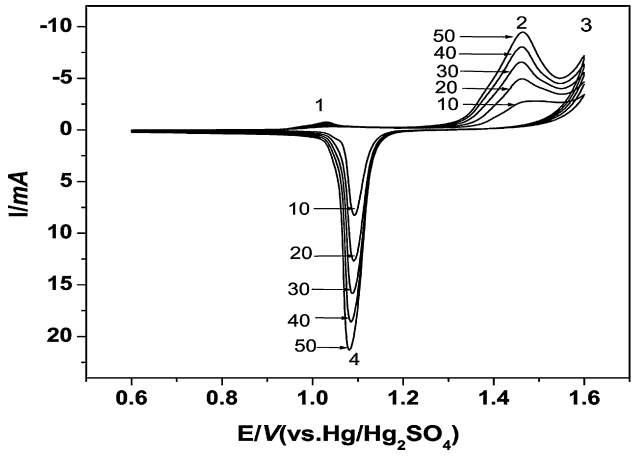

Fig. 10. Cyclic voltammograms for a Pb–0.0112 wt.% La electrode in 1.28 g cm^{-3} H_2SO_4 for the 10th, 20th, 30th, 40th, and 50th cycle (scan rate = 1 mV s^{-1}).

the PbO_2 membrane. The alloys with La contents of 0.00600 and 0.0540 wt.% were more effective.

3.3. Cyclic voltammetry

Fig. 10 illustrates the cyclic voltammograms for Pb–0.0112 wt.% La electrodes in 1.28 g cm^{-3} H_2SO_4 for the 10th, 20th, 30th, 40th and 50th cycle performed between 0.6 and 1.6 V at a sweep rate of 1 mV s^{-1}. The cyclic voltammetry (CVs) of other electrodes are not shown since they have similar shapes to those in Fig. 10. In the positive sweep, three anodic peaks: 1, 2 and 3 are observed, which correspond to the formation of Pb(II) oxides, PbO_2 and oxygen evolution, respectively [21]. In the negative sweep, the cathodic peak 4 corresponds to the reduction of PbO_2.

It can be seen from Fig. 10 that there is a good linear relationship between the area of the peaks (1,2,3 and 4) and the cyclic number (N). Zhou suggested that the enlarged peak current originates from the increased surface area due to the formation of a porous film during the cyclic process [22].

Table 3 lists the cathodic reduction charges (Q_c) of peak 4 in the cyclic voltammograms for Pb–La alloy electrodes at different cycles and the growth rates of Q_c of the electrodes. The results show that the growth rate of Pb–0.00600 wt.% La is the least, followed by Pb–0.0112 wt.% La and Pb–0.0540 wt.% La, while Pb–0.0195 wt.% La and pure Pb have the same higher growth rate value of 0.0027. The results indicate that the addition of La can decrease the growth rate

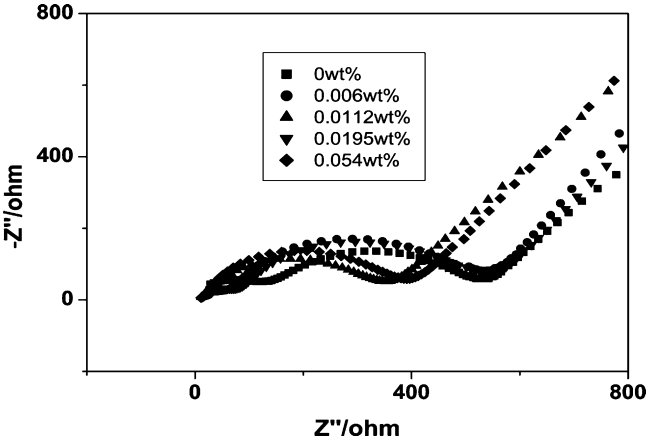

Fig. 11. Nyquist plots of Pb alloy electrodes with different amounts of La in 1.28 g cm^{-3} H_2SO_4 at 0.9 V.

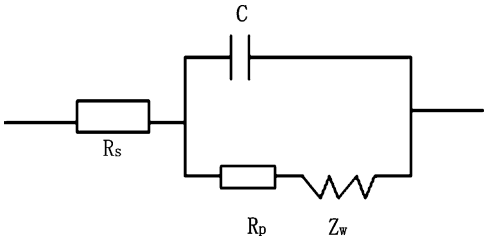

Fig. 12. The equivalent circuit of Fig. 11.

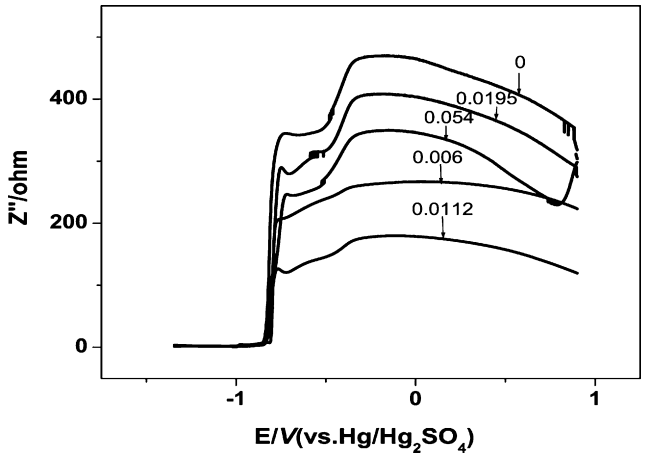

Fig. 13. Z vs. E plots of the anodic films formed on Pb and Pb–La alloys at 0.9 V in 1.28 g cm^{-3} H_2SO_4 solution for 1 h (scan rate = 1 mV s^{-1}, f = 1000 Hz).

of the anodic corrosion PbO_2 layer, especially with the 0.00600 wt.% La content. Addition of La possibly changes the microstructure of the alloys and the morphology of $PbSO_4$ crystals.

3.4. Study of PbO growth

When the potential of the anodic oxidation of lead in sulfuric acid solution is located in the PbO potential region (−0.40–0.95 V), an anodic film with a complex composition can be obtained, i.e., Pb/PbO/3PbO·$PbSO_4$·H_2O/PbO·$PbSO_4$/$PbSO_4$, with anodic Pb(II) film as the major component. Since the resistivity of the PbO crystal is quite high (at about 10^{11} Ω cm), the high resistance of the anodic Pb(II) film greatly influences the deep-charge/discharge performance of the battery. In our present experiment, the electrodes were kept at 0.9 V for 1 h before measurements were made. As

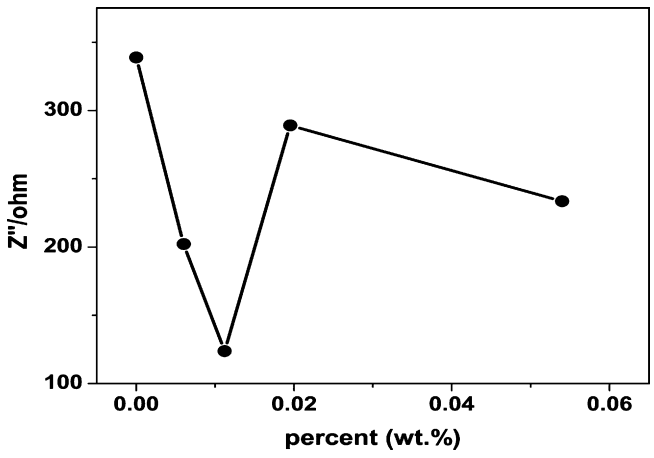

Fig. 14. Relationship between Z and La weight percent at −0.75 V.

Table 3
Reduction charges of the peak $d(PbO_2/PbSO_4)$, Q_c.

Cycles/N	Q_c (C cm^{-2})				
	Pb	Pb–0.006 La	Pb–0.0112 La	Pb–0.0195 La	Pb–0.054 La
10	0.053	0.032	0.046	0.051	0.043
20	0.087	0.057	0.075	0.083	0.074
30	0.113	0.080	0.096	0.108	0.095
40	0.138	0.101	0.121	0.133	0.120
50	0.161	0.122	0.148	0.151	0.146
Growth rate (C cm^{-2} N)	0.0027	0.0023	0.0025	0.0027	0.0025
R	0.998	0.999	0.999	0.997	0.997

shown in Fig. 11 the electrochemical impedance plot of the pure Pb electrode is similar to that of the Pb–La electrodes. The plots show a semicircular region at high frequency and a linear region at low frequency, which are associated with a charge transfer step and a diffusion-controlled step, respectively. Consequently, the electrochemical impedance behavior shown in Fig. 11 can be represented by a simple equivalent circuit (Fig. 12). R_s is the electrolyte resistance, and C is the capacity of the electric double-layer. R_p and Z_w are the resistances of the anodic film and the Warburg impedance, respectively. The results are listed in Table 4.

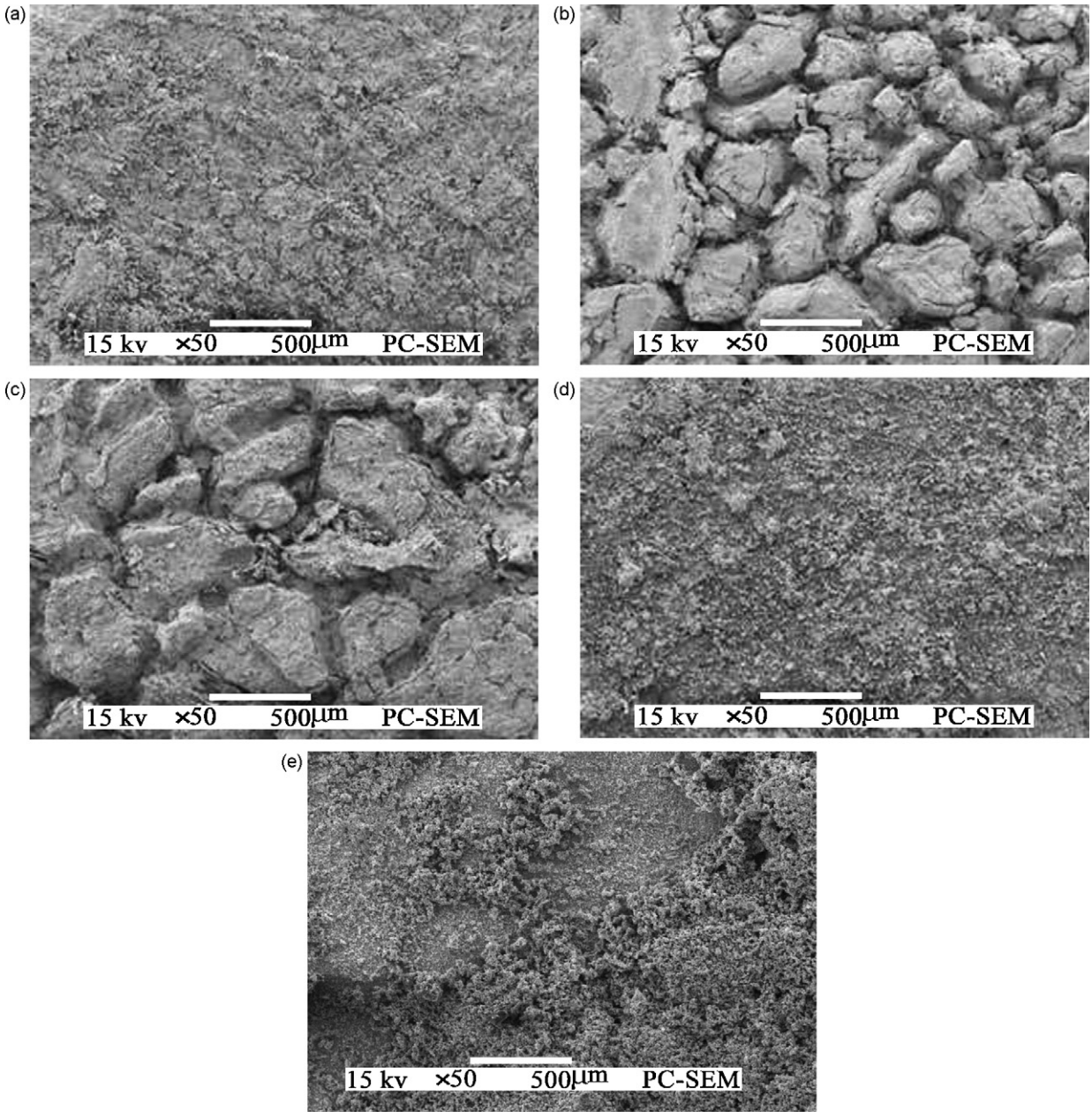

Fig. 15. SEM images of the corrosion layer of Pb and Pb–La alloy electrodes with different La amounts: (a) La = 0 wt.%; (b) La = 0.00600 wt.%; (c) La = 0.0112 wt.%; (d) La = 0.0195 wt.%; (e) La = 0.0540 wt.%.

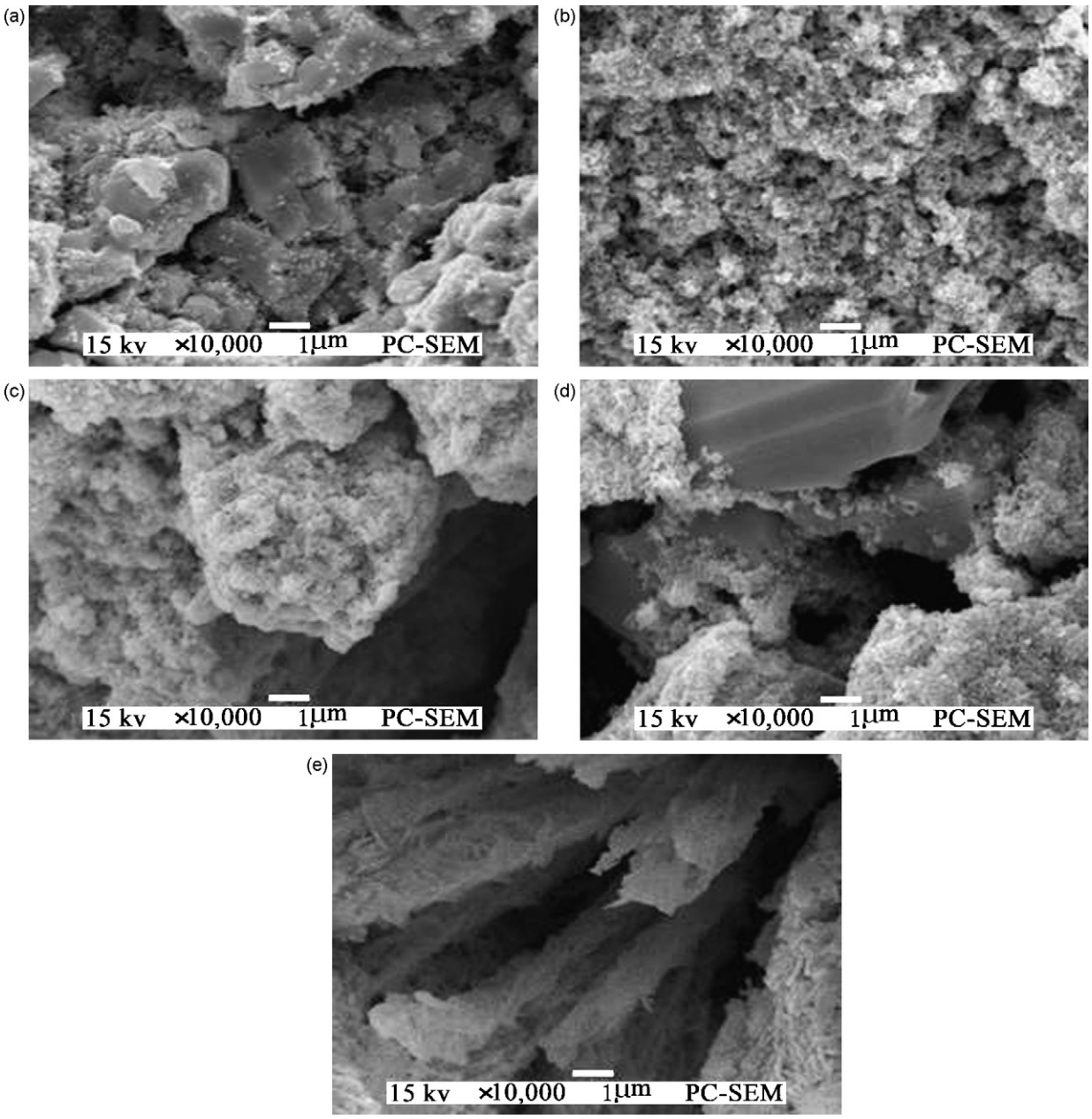

Fig. 16. SEM images of the corrosion layer of Pb and Pb–La alloy electrode with different La amounts: (a) La = 0 wt.%; (b) La = 0.00600 wt.%; (c) La = 0.0112 wt.%; (d) La = 0.0195 wt.%; (e) La = 0.0540 wt.%.

It can be seen that the resistance of the anodic film on the Pb electrode is much higher than that on the Pb–La electrodes. The possible reasons are: (i) the amount of anodic Pb(II) film formed on the surface of the Pb electrode is much greater than that on the Pb–La electrodes; (ii) the addition of La reduces the resistance of the anodic Pb(II) film and then increases the conductivity of passive film formed on Pb–La alloy electrodes. The anodic Pb(II) film formed on the electrodes with 0.006 and 0.0540 wt.% La is less than for pure lead.

Table 4
Resistance of anodic films formed on Pb alloy electrodes with different amount of La.

	La (wt.%)				
	0.00	0.006	0.0112	0.0195	0.054
R_s (Ω)	28	25.6	22.1	22.4	21.3
R_p (Ω)	647	469	314	516	336
Z_w (Ω) × e^{-2}	0.24	0.13	0.23	0.16	0.21
C (F) × e^{-2}	1.24	0.3	0.18	0.56	0.11

The variation of the impedance of the anodic film with a negative linear potential sweep (LSV) has been measured by ac voltammetry. Fig. 13 shows the Z (real part of the impedance) vs. E plots of the anodic films formed on Pb electrodes with different amounts of La. It can be observed that the impedance drops suddenly at a potential of about −0.75 V, which corresponds to the transformation of Pb(II) oxides to Pb, with resultant good conductivity. It can be seen from Fig. 14 that the Z value of the Pb electrode is higher than that of Pb–La alloys. This suggests that the addition of lanthanum may reduce the resistivity of the anodic Pb(II) film and then increase the conductivity of passive film formed on Pb–La alloys. It can also be seen that the Z values of electrodes with 0.00600, 0.0112 and 0.0540 wt.% La are smaller. This result is consistent with the results of electrochemical

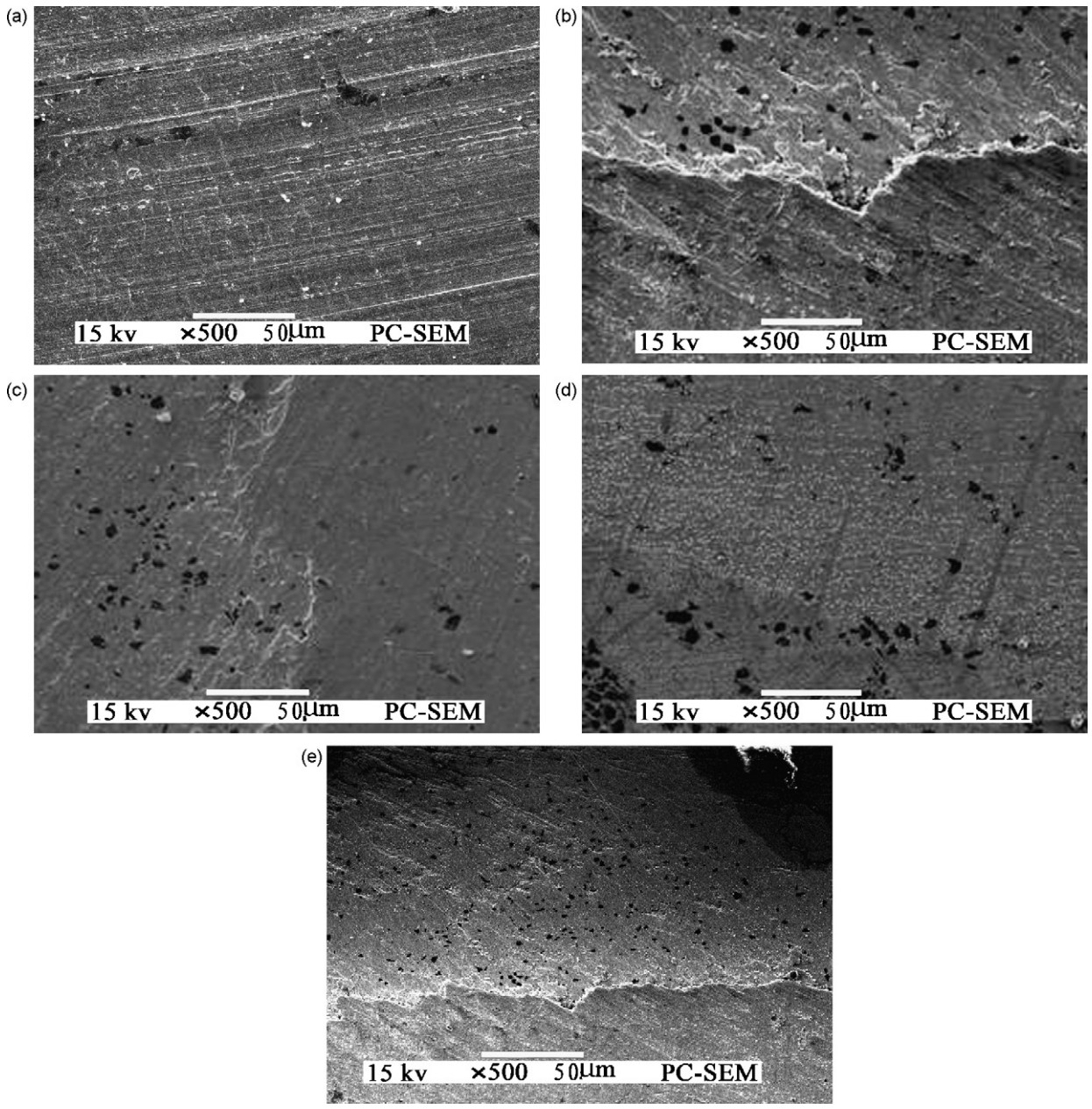

Fig. 17. Cross-sectional views of the corrosion layer of Pb and Pb–La alloy electrodes with different La amounts: (a) La = 0 wt.%; (b) La = 0.00600 wt.%; (c) La = 0.0112 wt.%; (d) La = 0.0195 wt.%; (e) La = 0.0540 wt.%.

impedance measurements and linear sweep voltammetry experiments.

3.5. SEM micrographs of the corrosion test

Fig. 15 provides SEM images of the corrosion layer of Pb–La alloy electrodes. It can be seen that the corrosion layers are almost the same as pure Pb and Pb–0.0195 wt.% La alloys, and that they are uniform and compact; this may be the reason that Pb–0.0195 wt.% La and pure Pb electrodes have similar electrochemical behavior, as shown above. This compact form may weaken the adhesion between the grid and the active material. The corrosion layer of other alloys is porous, which may reduce the selectivity of the corrosion layer, leading to the corrosion attacking more easily. The porous structure is favorable to the active materials sitting in the apertures to contact the grid surface intimately with the effective. The SEM images (Fig. 16) of the corrosion layer with higher magnification reveal that the corrosion products of pure Pb and Pb–0.0195 wt.% La alloys are composed of irregular-shaped agglomerates which consist of fine, rhombic crystals. The corrosion products of alloys with other amounts of La are loose and porous. The corrosion product of Pb–0.0540 wt.% La alloy is exceptional, consisting of loose, dendritic crystals growing out from the base of the alloy. It could be concluded that the addition of the correct amount of lanthanum changed the structure of the corrosion product.

Fig. 17 shows the cross-sectional views of the alloys. A clear boundary is observed between layers in the alloys with 0.00600, 0.0112 and 0.0540 wt.% La. No internal boundary is observed in pure Pb and Pb–0.0195 wt.% La alloys but a larger number of pores are visible. The corrosion layers of alloys with 0.00600, 0.0112 and 0.0540 wt.% La, presented in Fig. 15 are clear. This indicates that the corrosion layer of pure Pb and Pb–0.0195 wt.% La alloys is too compact and thin to combine with the active material.

4. Conclusion

1. The addition of La can inhibit the oxygen evolution reaction on the surface of Pb alloys electrodes, and adding 0.00600 and 0.0540 wt.% La cause a more effective inhibition compared with 0.0112 or 0.0195 wt.%.
2. The results of LSV, CV and electrochemical impedance spectroscopy (EIS) indicated that the addition of La can inhibit the growth of the anodic Pb(II) oxides and PbO_2 film.
3. The corrosion product on the Pb–La alloys with 0.00600, 0.0112 and 0.0540 wt.% La is so loose and porous that the active materials can easily sit in the apertures to contact the grid surface intimately with the effective.

References

[1] X.-G. Hu, X.-X. Mao, Chin. J. Power Sources 34 (2000) 230–237.
[2] M. Kniveton, J. Power Sources 96 (2001) 140–144.
[3] K.R. Bullock, J. Electrochem. Soc. 142 (1995) 1726–1731.
[4] R. David Prengaman, J. Power Sources 53 (1995) 207–214.
[5] G.J. May, J. Power Sources 59 (1996) 147–151.
[6] R. David Prengaman, J. Power Sources 95 (2001) 224–233.
[7] D.W.H. Lambert, J.E. Manders, R.F. Nelson, K. Peters, D.A.J. Rand, M. Stevenson, J. Power Sources 88 (2000) 130–147.
[8] Z.S. Liu, S.X. Dou, J. Power Sources 59 (1996) 123–129.
[9] M. Metikos-Hukovic, R. Babic, S. Brinic, J. Power Sources 64 (1997) 13–19.
[10] H. Tokiyoshi, S. Kazuya, T. Masami, J. Power Sources 85 (2000) 44–48.
[11] D. Pavlov, B. Monakhov, M. Maja, N. Pennazzi, J. Electrochem. Soc. 136 (1989) 27–33.
[12] D. Slavkov, B.S. Haran, B.N. Popov, F. Fleming, J. Power Sources 112 (2002) 199–208.
[13] L.T. Lam, N.P. Haigh, D.A.J. Rand, J. Power Sources 88 (2000) 11–17.
[14] E. Hilali, L. Bouirden, Ann. Chim. Sci. Mater. 25 (2000) 91–100.
[15] H.-Y. Chen, S. Li, D. Shu, W.S. Li, C.L. Dou, Q. Wang, J. Power Sources 168 (2007) 79–89.
[16] Y.B. Zhou, C.X. Yang, W.F. Zhou, H.T. Liu, J. Alloys Compd. 365 (2004) 108–111.
[17] H.T. Liu, X.H. Zhang, Y.B. Zhou, C.X. Yang, W.F. Zhou, Mater. Lett. 57 (2003) 4597–4600.
[18] H.T. Liu, J. Yang, H.H. Liang, J.H. Zhuang, W.F. Zhou, Electrochemistry 6 (3) (2000) 265–271.
[19] H.T. Liu, C.X. Yang, H.H. Liang, J. Yang, W.F. Zhou, Electrochemistry 7 (4) (2001) 439–444.
[20] H.T. Liu, X.H. Zhang, J. Yang, C.X. Yang, W.F. Zhou, Acta Chim. Sin. 600 (4) (2002) 643–646.
[21] Y.-B. Zhou, et al., J. Alloys Compd. 365 (2004) 108–111.
[22] W.-F. Zhou, X.-L. Cheng, Acta Chim. Sin. 43 (1985) 333–339.